PSFC/JA-10-61

Linearly Polarized Modes of a Corrugated Metallic Waveguide

Kowalski, E.J., Tax, D.S., Shapiro, M.A., Sirigiri, J.R., Temkin, R.J., Bigelow, T.S.*, Rasmussen, D.A.*

* U.S. ITER Project Office and Oak Ridge National Laboratory, Oak Ridge, TN 37831

2010

Plasma Science and Fusion Center
Massachusetts Institute of Technology
Cambridge MA 02139 USA

Linearly Polarized Modes of a Corrugated Metallic Waveguide

Elizabeth J. Kowalski*, David S. Tax*, Michael A. Shapiro*, Jagadishwar R. Sirigiri*, Richard J. Temkin*,
Timothy S. Bigelow†, David A. Rasmussen†

*Massachusetts Institute of Technology, Plasma Science and Fusion Center, Cambridge, MA 02139, USA
†US ITER Project Office and Oak Ridge National Laboratory, Oak Ridge, TN 37831, USA

Abstract—**High power, high frequency microwave radiation can be transmitted with very low loss in oversized corrugated metallic waveguide. We derive a linearly polarized (LP_{mn}) mode basis set for these waveguides for the special case of quarter wavelength depth corrugations. We also show the relationship between the LP_{mn} modes and the conventional modes (HE_{mn}, EH_{mn}, TE_{0n}, TM_{0n}) of the corrugated guide. The loss in a gap or equivalent miter bend in the waveguide is calculated for single mode and multi-mode propagation on the line. In the latter case, it is shown that modes of the same symmetry interfere with one another, causing enhanced or reduced loss, depending on the relative phase of the modes. If two modes with azimuthal (m) indeces that differ by one propagate in the waveguide, the resultant centroid and the tilt angle of radiation at the guide end are shown to be related through a constant of the motion. These results should be useful in describing the propagation of high power, linearly polarized radiation in these overmoded, corrugated waveguides.**

I. Introduction

An important problem in research with high power, high frequency coherent microwave radiation is the transmission of the radiation from the source to the application. In recent years, rapid advances in the development of gyrotrons have made available sources of continuous power at levels in the megawatt range at frequencies of up to 170 GHz. The radiation from gyrotrons is often transported long distances, many tens of meters, before being launched for plasma heating. The transmission lines ordinarily used in these applications are over-sized corrugated metallic waveguides. These waveguides provide low loss and low mode conversion. The metallic wall helps to prevent accidental loss of radiation. Other major uses of these corrugated waveguides include transmission lines for plasma diagnostics, radar, materials heating and spectroscopy.

The theory for modes of corrugated metallic waveguides has been previously developed [1], [2], [3], [4]. The original application of corrugated waveguides was in the development of horn antennas, but recent applications of straight corrugated waveguide have led to a large literature devoted to that specific topic. A set of eigenmodes has been derived for corrugated metallic waveguide, consisting of hybrid modes, both HE_{mn} and EH_{mn} modes, plus the TE_{0n} and TM_{0n} modes [5], [6], [7]. The fundamental mode of corrugated waveguide, the HE_{11} mode is linearly polarized. However, the hybrid modes are, in general, not linearly polarized. The purpose of this paper is to develop a set of linearly polarized eigenmodes (LP_{mn}) for corrugated metallic waveguide. Since gyrotron beams are

linearly polarized, the LP_{mn} mode set has advantages for describing this radiation. We also develop a number of useful results for the propagation of LP_{mn} modes in corrugated metallic waveguide.

The corrugated waveguides consist of hollow metallic cylinders where the inner wall has periodic wavelength-scaled grooves, as depicted in Figure 1. Figure 1 also shows the parameters of the waveguide and the coordinates used in describing the modes. The fundamental mode of the corrugated waveguide, the HE_{11} mode, has less attenuation than the fundamental modes for equivalent smooth-wall cylindrical and rectangular waveguides. This effect is reviewed for frequencies from 1-10 GHz in [1] and for the 100 GHz range in [3]. Overmoded corrugated waveguides have extremely low losses at high frequencies, even for higher order modes [8], [9]. The attenuation for a corrugated guide scales inversely with the cube of the radius to wavelength ratio, a/λ. The loss in straight waveguide sections is so low that we will omit discussion of that loss in this paper; the loss is discussed at length in [5]. However, if the guide size (a/λ) is too large for the application at hand, power will be lost due to misalignment and fabrication errors.

The results obtained in this paper will be specialized to the case of a quarter-wavelength groove depth, $d = \lambda/4$, which is the optimum depth for the lowest attenuation in the waveguide. We will also specialize our analysis to waveguides with large values of a/λ. An important application that is currently under development is the transmission line for the Electron Cyclotron Heating system for the ITER tokamak, which will have twenty-four one megawatt gyrotrons at 170 GHz. Each gyrotron will have a transmission line that is over one hundred meters long [10]. These transmission lines have been designed with a corrugation depth, $d = \lambda/4$, of 0.44 mm and a radius
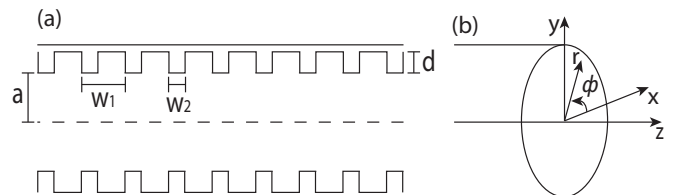

Fig. 1. (a) A cylindrical corrugated waveguide with a radius of a. The corrugations are defined by w_1, w_2, and d. For low loss characteristics the corrugation depth is $d = \lambda/4$. (b) An illustration of the variables in the cylindrical geometry.

of a =31.75 mm, such that a/λ =18 [11]. In this paper, we will use this case for illustrating some important examples.

Over-moded corrugated waveguides ideally operate only in the fundamental HE_{11} mode, but higher order modes (HOMs) also propagate along the line with low losses. For many high power, high frequency experiments, such as ITER, gyrotrons are used to produce Gaussian (TEM_{00}) beam inputs for the transmission line system. Ideally, the Gaussian beam couples to and propagates as the fundamental HE_{11} mode in the transmission line, with 98% theoretical coupling [12]. However, experimentally realistic gyrotron inputs are imperfect Gaussian beams and can be injected into the transmission line system with tilt and/or offset, causing the excitation of HOMs on the over-moded transmission line [13]. These HOMs are supported in the line and will propagate with small attenuation. Interference effects caused by HOMs, that is, by the presence of more than one mode on the transmission line, are considered in this paper.

In Section II of this paper, we derive the set of LP_{mn} modes of a circular, corrugated, metallic waveguide with quarter wave corrugations. The derivation is complete, but it is shortened by taking advantage of prior work in deriving the hybrid modes. In Section III, we show the relationship of the set of LP_{mn} modes to the usual hybrid mode set. Since each set of modes can form a basis set, they must be related. The results are illustrated by the construction of the lowest order LP_{mn} modes, including the LP_{11} and the LP_{21} modes, from the hybrid modes. In Section IV, we derive the loss in power of a single LP_{mn} mode propagating through a gap in the waveguide. The result is also analogous to the loss due to a miter bend, a common transmission line component. In Section V, we discuss the gap loss for a mixture of LP_{mn} modes. For modes of the same azimuthal symmetry, the relative phase of the modes is found to play a major role in the gap loss. In Section VI, we consider two modes propagating together on the transmission line which is terminated. In this case, we find that modes of different symmetry interfere at the end of the waveguide, causing the centroid of power to be offset and/or the fields to radiate with a tilt angle. A constant of the motion involving the tilt and offset is derived. Section VII is a discussion.

The results derived in this paper should be useful in planning corrugated waveguide transmission lines for high power microwave systems and in analyzing the properties of the waveguides.

II. DESCRIPTION OF LP_{mn} MODES

In this section, we show that linearly polarized, LP_{mn}, modes form a basis set for metallic corrugated waveguides with corrugations of depth, $d = \lambda/4$. These modes are particularly convenient for use in treating the transmission of high power radiation from gyrotrons since gyrotrons produce linearly polarized microwave beams. We also will show the relationship of the LP_{mn} mode basis set to the conventional hybrid mode basis set of HE, EH, TE, and TM modes [5], [6], [7], [14], [15], [16]. The fields of the hybrid modes in over-moded corrugated circular waveguides are defined readily in

the literature in cylindrical coordinates [5], [13]. Though the hybrid modes create a basis set, a discrepancy can easily arise between the polarization of the beam and the defined modes of the beam if the modes are matched while considering only field intensity and not field polarization. The use of LP modes reduces the possibility of polarization discrepancy for common applications that use a linearly polarized gyrotron input. Since LP modes form a basis set, they may also be used to construct other beams as well, a necessity when considering imperfections of the input which can cause elliptically polarized modes in much smaller quantities.

The field in a corrugated waveguide can be split into two parts, the field of the propagating modes which exists for $r < a$ and the field that exists in the corrugation grooves where $a < r < a+d$. In the grooves, a standing wave pattern forms which imposes a wall impedance on the boundary $r = a$ for the propagating wave which exists at $r < a$. Within the corrugation, at $r = a+d$, $E_z = 0$ and H_ϕ is maximized. These conditions lead to the wall impedance in the z direction as,

$$Z_z = \frac{E_z(r = a)}{H_\phi(r = a)} = Z_0 \tan(kd), \tag{1}$$

where k is the wavenumber and Z_0 is defined by the corrugation widths,

$$Z_0 = -j\frac{w_1 - w_2}{w_1}\sqrt{\frac{\mu_0}{\varepsilon_0}} \tag{2}$$

(see Figure 1 for parameter definitions) [5], [6]. For the case considered here $d = \lambda/4$, so $Z_z = \infty$, and $H_\phi(r = a) = 0$. This condition extends to the transverse electric field components, such that $E_\phi(r = a) = 0$ and $E_r(r = a) = 0$.

To satisfy the linearly polarized field stipulation, the transverse electric field for $r < a$ is expressed in Cartesian coordinates. Through coordinate definitions,

$$E_y = E_r \sin \phi + E_\phi \cos \phi. \tag{3}$$

$$E_x = E_r \cos \phi - E_\phi \sin \phi. \tag{4}$$

To polarize in the $\hat{y}$ direction, E_x must be zero, which implies that $E_r = f(r, \phi, z) \sin \phi$, and $E_\phi = f(r, \phi, z) \cos \phi$. These forms satisfy the wave equations for cylindrical coordinates and boundary conditions imposed by the corrugations, so long as $f(a, \phi, z) = 0$. Therefore, $E_y = f(r, \phi, z)$ and the boundary condition that must be satisfied for linearly polarized modes is $E_y(r = a, \phi, z) = 0$. This extrapolation of E_y is similar to the definition of LP modes for dielectric waveguides, as in [17]. One main difference between the two different waveguides is the boundary conditions; whereas dielectric guides have finite fields at the wall, the metallic guides considered here have $E_y = 0$ at the wall of the guide.

Solving for the fields in the waveguide requires E_y to satisfy the wave equation, as well. Though the electric field is discussed in Cartesian coordinates to satisfy the linearly polarized condition, it is more convenient to use cylindrical variables to express the function, such that

$$\frac{\partial^2 E_y}{\partial r^2} + \frac{1}{r}\frac{\partial E_y}{\partial r} + \frac{1}{r^2}\frac{\partial^2 E_y}{\partial \phi^2} + \frac{\partial^2 E_y}{\partial z^2} + \frac{\omega^2}{c^2}E_y = 0. \tag{5}$$

Assuming a z-dependence of $e^{-jk_z z}$ and a ϕ-dependence of $\cos(m\phi)$ or $\sin(m\phi)$ the wave equation is reduced to

$$r^2 \frac{\partial^2 E_y}{\partial r^2} + r \frac{\partial E_y}{\partial r} + ((k_r r)^2 - m^2) E_y = 0. \qquad (6)$$

which is the Bessel function differential equation, where $k_r = \sqrt{(\omega^2/c^2 - k_z^2)}$. The Bessel function of the first kind is chosen to satisfy finite electric field conditions, such that

$$E_y(r, \phi, z, t) = A J_m(k_r r) e^{j(\omega t - k_z z)} \left\{ \begin{array}{c} \cos(m\phi) \\ \sin(m\phi) \end{array} \right\}, \quad (7)$$

where A is a constant and either sinusoidal dependence on ϕ is possible. The boundary condition $E_y(a, \phi, z) = 0$ requires that $k_r = X_{mn}/a$, where X_{mn} is the nth zero of the mth Bessel function. Through Maxwell's equations, the dominate field components for LP_{mn} modes are

$$E_{y,mn}(r, \phi) = A J_m \left(\frac{X_{mn} r}{a} \right) \left\{ \begin{array}{c} \cos(m\phi) \\ \sin(m\phi) \end{array} \right\}, \quad (8)$$

$$H_{x,mn}(r, \phi) = \frac{-A k_z}{\omega \mu_0} J_m \left(\frac{X_{mn} r}{a} \right) \left\{ \begin{array}{c} \cos(m\phi) \\ \sin(m\phi) \end{array} \right\}, \quad (9)$$

where the functional dependence of E and H on z and t, $e^{j(\omega t - k_z z)}$, has been dropped for simplicity. The longitudinal components, E_z and H_z, and the transverse magnetic field in the y-direction, H_y, are nonzero, but negligible by a factor of λ/a. The transverse electric field in the x-direction is defined due to the linear polarization condition as $E_x = 0$.

The odd and even LP_{mn} modes are defined with a perpendicular electric field as

$$\vec{E}_{mn}^{\perp}(r, \phi) = \hat{y} A J_m \left(\frac{X_{mn} r}{a} \right) \left\{ \begin{array}{cc} \cos(m\phi) & \text{(odd)} \\ \sin(m\phi) & \text{(even)}. \end{array} \right. \quad (10)$$

To create an orthonormal basis set, a normalization factor is calculated

$$N_{mn} = \int_0^a \int_0^{2\pi} \left(E_{mn}^{\perp}(r, \phi) \right)^2 r \, d\phi dr. \qquad (11)$$

For LP_{0n} (HE_{1n}) modes, this normalization evaluates to

$$N_{0n} = A^2 \pi a^2 J_1^2(X_{0n}), \qquad (12)$$

and for all other LP_{mn} modes, where $m \neq 0$,

$$N_{mn} = A^2 \frac{\pi a^2}{2} J_{m-1}^2(X_{mn}). \qquad (13)$$

With this factor,

$$u_{mn} = E_{mn}^{\perp}/\sqrt{N_{mn}}, \qquad (14)$$

such that u_{mn} is a simple way to express the normalized mode.
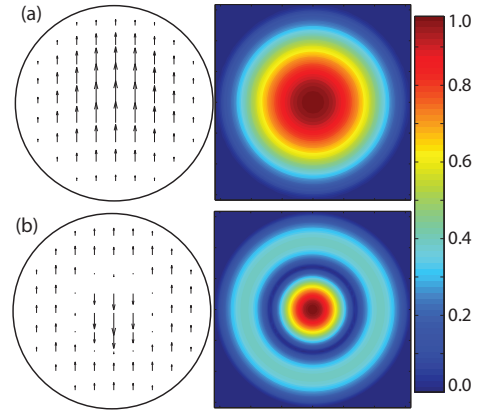

Fig. 2. Field vector and magnitude plots for (a) LP_{01}/HE_{11} and (b) LP_{02}/HE_{12}. (Amplitudes are normalized.)
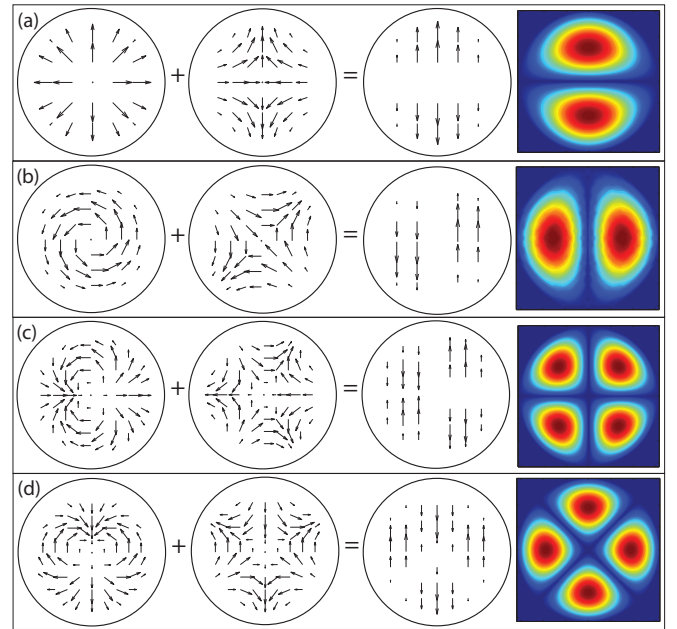

Fig. 3. Field vector plots demonstrating the construction of LP modes from TE, TM, and HE modes. The added modes have identical propagation constants. (a) $TM_{02} + HE_{21}$ rotated $45° = LP_{11}^{(e)}$; (b) $-TE_{01} + HE_{21} = LP_{11}^{(o)}$; (c) EH_{12} rotated $-90° + HE_{31}$ rotated $-90° = LP_{21}^{(e)}$; (d) EH_{12} rotated $180° + HE_{31} = LP_{21}^{(o)}$.

III. RELATIONSHIP BETWEEN HYBRID AND LP_{mn} MODES

Any wave propagating in the corrugated metallic waveguide can be projected onto an orthonormal basis set of modes. Both the hybrid modes and the LP_{mn} modes form such a basis set. Here, we indicate the relationships between these two basis sets and show how the LP_{mn} modes can be constructed from the hybrid mode basis set.

Figure 2 illustrates the vector field and magnitude plots of the electric field for two common LP_{mn} modes. Note that the HE_{1n} modes are the same as the LP_{0n} modes. Therefore, the HE_{1n} notation will be kept in order to agree with the existing literature; this assignment is useful for discussing the fundamental HE_{11} mode.

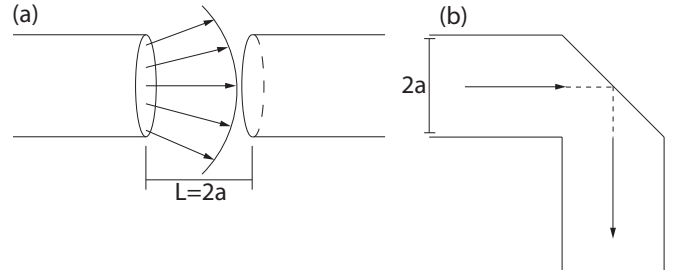LP_{mn} modes can be constructed through the addition

Fig. 4. (a) A radially symmetric gap with length $L = 2a$. (b) A miter bend with a radius of a that can be modeled using equivalent gap theory, as described in the text.

of HE_{mn}, EH_{mn}, TE_{0n}, or TM_{0n} modes with the same propagation constants (degenerate modes). Table I lists these degenerate modes. Figure 3 illustrates, for a few LP modes, how the addition of hybrid modes can form LP_{mn} modes. The first two examples, the LP_{11} modes, were previously described in [9]. Through the field vector plots, Figure 3 demonstrates this relationship between LP modes and HE, EH, TE, and TM modes. For example, the $LP_{11}^{(e)}$ mode can be constructed by adding the TM_{02} mode and the HE_{21} mode, rotated by $45°$ as seen in Figure 3a. When adding these modes, the $\hat{x}$-components of the field cancel while the $\hat{y}$-components add, resulting in a $\hat{y}$-directed linearly polarized field. All three of these modes are characterized by the Bessel function zero $X_m = 3.832$ and, therefore, have the same beat wavelength with the HE_{11} mode. Since both sets of modes are basis sets, it is possible to use either set to describe a linearly polarized beam in a waveguide. However, it is necessary to account for HE, EH, TE, and TM modes that result in combinations (like those listed above) to preserve linear polarization. Due to this restriction, it is more convenient to consider the LP mode basis set for analysis in corrugated cylindrical waveguides with linearly polarized experimental inputs.

IV. GAP LOSS FOR PURE MODE INPUTS

Most waveguide transmission lines are dominated by long, straight sections of waveguide which have negligible loss when $a/\lambda \gg 1$ [5]. However, a practical waveguide system must have waveguide gaps, bends, and switches in which the wave propagates a distance without a confining wall. Losses in these gaps often dominate the total loss of the line. In this section, we calculate the power loss for an arbitrary LP_{mn} mode due to a gap in straight waveguide. The exercise computes the field and mode amplitudes of a wave which radiates from the end of a transmitting waveguide through a gap consisting of free space and couples into a receiving waveguide after the gap. When the length of the gap, L, is equivalent to the diameter of the waveguide (that is $L = 2a$), the gap geometry is an approximate 2-dimensional model of a $90°$ miter bend in the

Mode	X_{mn}	Degenerate modes
LP_{01}	2.405	HE_{11}
$LP_{11}^{(o)}$	3.832	TE_{01}, HE_{21}
$LP_{11}^{(e)}$	3.832	TM_{02}, HE_{21}
LP_{21}	5.136	HE_{31}, EH_{12}
LP_{02}	5.520	HE_{12}
LP_{31}	6.380	HE_{41}, EH_{22}
$LP_{12}^{(o)}$	7.016	TE_{02}, HE_{22}
$LP_{12}^{(e)}$	7.016	TM_{03}, HE_{22}
LP_{22}	8.417	HE_{32}, EH_{13}
LP_{03}	8.653	HE_{13}
LP_{32}	9.761	HE_{42}, EH_{23}
$LP_{13}^{(o)}$	10.17	TE_{03}, HE_{23}
$LP_{13}^{(e)}$	10.17	TM_{04}, HE_{23}

TABLE I
SELECT LP MODES WITH CORRESPONDING DEGENERATE MODES.

waveguide, as shown in Figure 4 [16]. Previously, the losses in a gap have been calculated for single mode inputs consisting of HE, TE, or TM modes [18] [19].

For LP_{mn} modes, the electric field in a gap is derived using the Fresnel Diffraction integral, an approach similar to [14], such that

$$E_{g,mn}^{\perp}(r,\phi,z) = \frac{jk}{z}e^{j\frac{kr^2}{2z}} \tag{15}$$
$$\iint E_i(r',\phi')e^{j\frac{k}{2z}[r'^2 - 2rr'\cos(\phi-\phi')]}r\,d\phi'dr'$$

where $E_i(r,\phi)$ defines the transverse electric field present at the end of the waveguide before the gap. In the single mode case, $E_i(r,\phi) = u_{mn}(r,\phi)$. Also, z is defined as the distance into the gap after the end of the waveguide. For an input consisting of a single normalized LP_{mn} odd mode, the electric field in the gap is

$$\vec{E}_{g,mn}^{\perp}(r,\phi,z) = \hat{y}\frac{j2\pi kA}{z\sqrt{N_{mn}}}e^{jm\frac{\pi}{2}}e^{j\frac{kr^2}{2z}}\cos(m\phi) \tag{16}$$
$$\int_0^a J_m\left(\frac{X_n r'}{a}\right)J_m\left(\frac{krr'}{z}\right)e^{j\frac{kr'^2}{2z}}r'dr'.$$

The integral with respect to ϕ has been solved using methods discussed in [20], while the integral with respect to r' must be solved numerically. Note that LP_{mn} even modes result in the same $\vec{E}_{g,mn}^{\perp}(r,\phi,z)$ as (16) with $\cos(m\phi)$ replaced by $\sin(m\phi)$.

Power loss in a specific mode occurs in the gap for two reasons. First, as a result of diffraction, some of the power exiting the transmitting waveguide lies outside of the receiving waveguide at $r > a$ and is lost, this is called truncation loss. Second, there is power which enters the receiving waveguide but couples to secondary modes instead of the original input mode. For large a/λ, all of the modes produced in the receiving waveguide will propagate down the waveguide, the coupling to other modes results in additional power loss when considering the original mode. This is called mode converstion loss.

In the equivalent miter bend, shown in Fig. 4(b), the power lost due to truncation is trapped inside of the bend. The power is distributed into very high order modes of the waveguide which do not propagate efficiently such that the power is dissipated through ohmic heating in long waveguide systems. The miter bend also suffers from mode conversion loss for the same reasons as in a gap. If the miter bend contains extensions
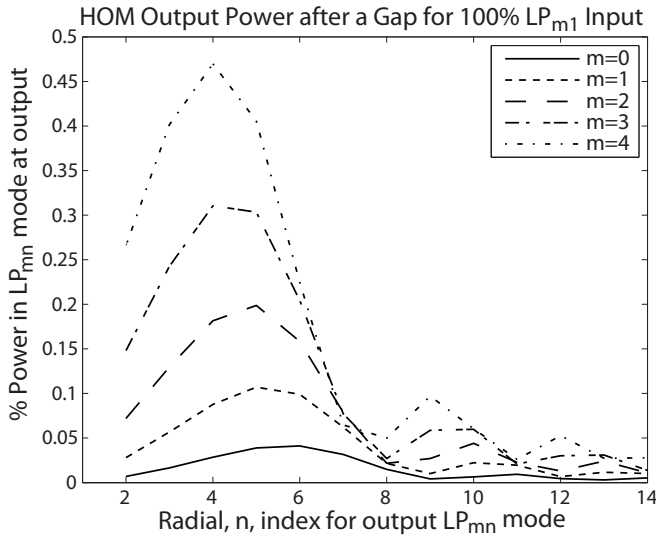
Fig. 5. The percent output of the power present in the LP_{mn} modes after a gap that results from a 100% LP_{m1} mode input, for $m = 0$ through $m = 4$. LP_{m1} mode power outputs (which are over 94%) have been cropped to show HOM content.

of the waveguide into the bend, the loss is reduced to one half of that of the equivalent gap [16].

For a/λ large, the power in the output port will consist primarily of power in the same mode (LP_{mn}) as was incident at the input port. Small amounts of power in other modes will also be present at the output port. These small amounts are illustrated for the case of LP_{m1} modes in Figure 5. Figure 5 shows the LP_{mn} mode content in the receiving guide due to a single LP_{m1} mode radiating from the transmitting guide through a gap of length $L = 2a$ and a system operating at 170 GHz with $a = 31.75$ mm. Results are shown for cases with $m = 0$ through 4. In these cases, over 94% of the power couples to the original input mode, less than 3% of the power is lost, and the rest of the power couples to HOMs with the same azimuthal, m, index, as shown in the figure.

A particular input mode will only result in output modes of the same azimuthal symmetry. For example, the case of 100% HE_{11} (LP_{01} in Figure 5) input results in 99.48% HE_{11} after the gap and 0.26% power lost in the gap. The remaining power goes into the HE_{1n} HOMs, with the largest percentages in HE_{16} (0.041%) and HE_{15} (0.039%), while HE_{12} is the seventh largest mode with 0.007% of the total power. Also, consider an input of 100% $\mathrm{LP}_{11}^{(o)}$, which has an output of 98.68% $\mathrm{LP}_{11}^{(o)}$, 0.67% of power lost to the gap, and the remaining power coupled into higher order $\mathrm{LP}_{1n}^{(o)}$ modes. In each of these cases, the input power is either lost in the gap or couples into modes with the same azimuthal symmetry as the original input mode.

V. GAP LOSS FOR MULTIPLE MODE INPUTS

In the previous section, we considered a single mode at the input port of the gap. In this section, we consider a multiple mode input. In this case, we must consider both the amplitudes of the modes and their phases. A multiple mode input follows the same procedure as a single mode input. The gap loss is calculated using (15), where the input electric field is now

defined as a summation of modes,

$$E_i(r, \phi) = \sum_m \sum_n \sqrt{A_{mn}} e^{j\theta_{mn}} u_{mn}(r, \phi), \qquad (17)$$

where A_{mn} and θ_{mn} indicate the relative power and phase of the input LP_{mn} modes. The output can also be expressed as a summation of each individual mode applied to Eq. (15) (as was done in the Eq. (16) in the previous section),

$$\vec{E}_g^\perp(r, \phi, L) = \sum_m \sum_n \sqrt{A_{mn}} e^{j\theta_{mn}} \vec{E}_{g,mn}^\perp(r, \phi, L). \quad (18)$$

The electric field in a gap for a multiple mode input is simply the summation of the electric field in a gap due to each individual mode input. After summing, the modal powers in the waveguide after the gap are calculated in the same way as the single mode case.

The phase difference between certain 2-mode input mode combinations causes variations in the power loss and mode content after the gap. The output HE_{11} power due to an input consisting of the HE_{11} and HE_{12} modes has a significant dependence on input phase, as shown in Figure 6(a) for gaps when $L = 2a$. Considering an input mode content of 98% HE_{11} and 2% HE_{12}, the power lost in HE_{11} ranges from 0.28% to 0.75%, corresponding to respective phase differences of 310° and 130°. The average loss in HE_{11} is 0.52%, the same value of loss as when HE_{11} is considered individually.

The dependence of power loss in a two mode system on the phase difference between the modes is seen in any combination of modes that has the same azimuthal (m) symmetry. For example, an input consisting of HE_{11} and HE_{13} will also have an output dependent on the phase between the two modes. This effect is seen in Figure 6(b). Though, the average loss in HE_{11} is still 0.52%, with a 2% HE_{13} content it may swing from 0.15% to 0.88%, depending on the input phase. This example treats modes of the same azimuthal symmetry (same m value). At the output port, a mode couples only to modes of the same azimuthal symmetry. Therefore, two modes of different azimuthal symmetry (different m values) will not interfere. For example, a two mode input consisting of an HE_{11} (LP_{01}) mode ($m = 0$) and $\mathrm{LP}_{11}^{(o)}$ mode ($m = 1$) produces an output that has no dependence on the relative phase of the modes and will always result in a 0.52% loss in the HE_{11} mode power.

A three or more mode input of the same azimuthal (m) symmetry will also result in a phase dependence. For example, an input consisting of HE_{11}, HE_{12}, and HE_{13}, will result in an output dependent on the phase relations between the modes. Results for varying values of HOM percentage and phases are shown in Figure 7, where the x-axis represents the total power in the combination of the HE_{12} and HE_{13} modes. The HE_{11} power loss is dependent on the phases of both modes as well as the percentage of power in each mode. A phase difference between HE_{11} and HE_{12} of 310° and HE_{13} of 120° causes the lowest possible power loss in HE_{11}, while phases of 130° and 300° in HE_{12} and HE_{13}, respectively, cause the largest possible power loss. Figure 7 shows the curves corresponding to these two extreme phase combinations. Both the absolute highest and lowest loss in HE_{11} power occur when 30% of the
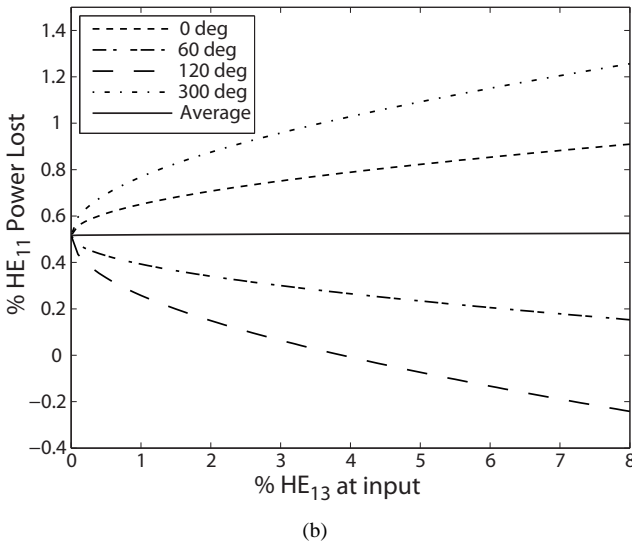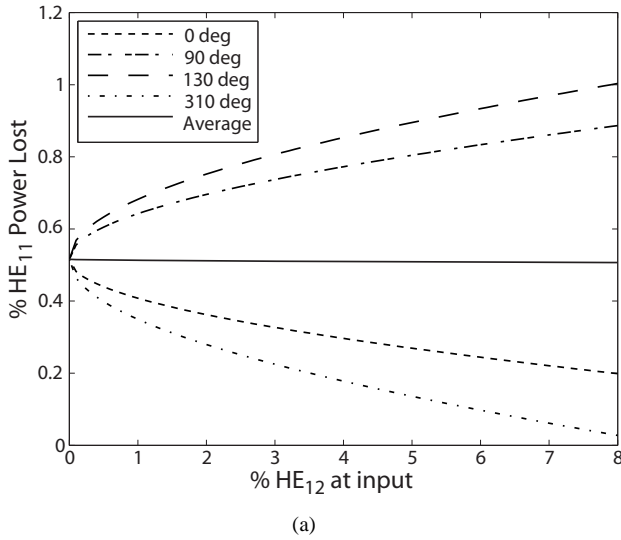
(a)

(b)

Fig. 6. For a two mode input at 170 GHz with $a = 31.75$ mm and $L = 2a$, the percent of (a) HE_{12} or (b) HE_{13} present in the input mode mixture vs. the percent loss in HE_{11} after the gap is plotted. Different phases of HE_{12} or HE_{13} have been chosen to show the full range of swing in the HE_{11} power loss. The average HE_{11} power loss is 0.52% for both cases.

Fig. 7. The power loss in a gap for HE_{11} vs. HOM content for a three mode input. The HOM content is split between HE_{12} and HE_{13}, and the largest and smallest HE_{11} power loss (due to HOM phase) is plotted for each mode split. The system is at 170 GHz with $a = 31.75$ mm.

Fig. 8. A wave radiating from the end of a waveguide at z_1 has a centroid of power with an offset, $x_0(z_1)$, and a tilt angle of propagation, $\alpha_x(z_1)$, as defined here.

HOM content is in HE_{12}, and 70% is in HE_{13}. In this case, a 2% HOM content may cause a swing in lost HE_{11} output power from 0.08% to 0.95% a swing that is larger than the result from 2% in HE_{12} or HE_{13} individually.

VI. CONSTANT OF THE MOTION FOR TILT AND OFFSET

At the termination of a transmission line, the fields may be radiated from the end of the guide to an antenna or directly into space. If a single mode is propagating on the line, the mode will reach the end of the line such that the fields are centered on the waveguide. The radiation pattern at the end of the guide can be calculated in the near and far fields. For a single mode, the direction of propagation will always be centered on and parallel to the waveguide axis. When two or more modes propagate down the transmission line, it is no longer true that the mode is, in general, centered on the waveguide axis. The fields will radiate f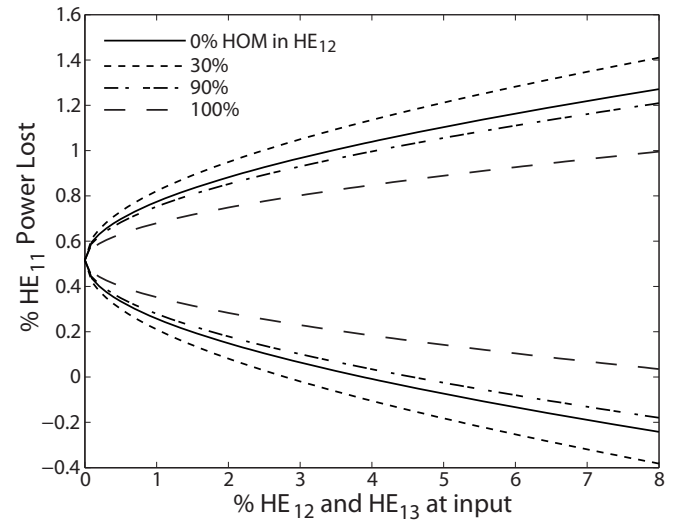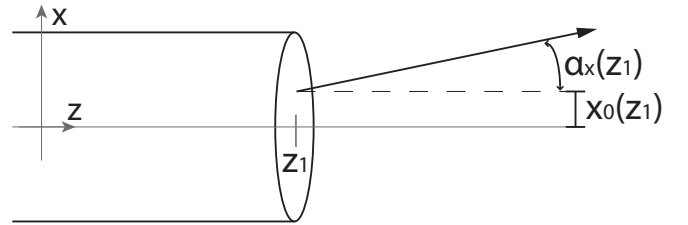rom the end of the waveguide, but the propagation angle will no longer, in general, be parallel to the waveguide axis. In this section, we derive a simple new result for the propagation of two modes that shows a relationship between the tilt and offset at the terminus of a corrugated waveguide transmission line.

The problem is illustrated in Figure 8, where the waveguide ends at a particular location of the z-axis, z_1. When a wave propagates outside of a waveguide, the centroid of power has a particular tilt angle, $\alpha_{x,y}(z)$, and offset, $x_0(z)$ and $y_0(z)$, from the center, as illustrated in Figure 8. These two propagation parameters (tilt angle and offset) define the wave after the waveguide and quantify the centroid of power.

The offset and tilt angle of propagation are controlled by the mode content of the wave in the waveguide. A two-mode content is characterized by two parameters, the relative amplitude and phase difference between the modes. For a pure mode leaving a waveguide, the centroid of the mode power is always on axis ($x_0, y_0 = 0$) and the mode has a constant flat phase front ($\alpha_{x,y} = 0$). However, when two modes propagate, the power centroid will generally be off-center from the axis and the phase front will be tilted by an angle.

A conservation theorem expressing the relationship between tilt and offset for two propagating LP_{mn} modes is derived. For

two modes, the electric field is defined as

$$E(x, y, z) = C_1(z)u_{m_1n_1}(x, y) + C_2(z)u_{m_2n_2}(x, y). \quad (19)$$

Here, C_p (where $p = 1, 2$ indicates the first or second mode of the system) is a complex variable indicating the amplitude and phase of the modes as

$$C_p(z) = \sqrt{A_p}e^{j(k_{z,p}z_1+\theta_p)}. \quad (20)$$

For the pth mode, A_p is the percentage of power in the mode, $k_{z,p}$ is the wavenumber in the $\hat{z}$-direction, and θ_p is the phase of the mode at $z_1 = 0$. Also, $u_{m_pn_p}(x, y)$ is the normalized field pattern of each mode as indicated in Eq. (14), with appropriate substitutions for r and ϕ to convert to the Cartesian coordinate system. The offset and propagation angle in the $\hat{x}$-direction are defined as

$$x_0(z_1) = \langle x(z_1) \rangle = \iint E^*(x, y, z_1)xE(z, y, z_1)dxdy, \quad (21)$$

$$\alpha_x(z_1) = \frac{\langle k_x(z_1) \rangle}{k} = \frac{-j}{k} \iint E^*(x, y, z_1)\frac{\partial E(x, y, z_1)}{\partial x}dxdy. \quad (22)$$

With the electric field defined for this problem, offset can be expressed as

$$x_0(z_1) = \iint xC_1C_2^*u_{m_1n_1}u_{m_2n_2}^*dxdy + \\ \iint xC_1^*C_2u_{m_1n_1}^*u_{m_2n_2}dxdy, \quad (23)$$

and reduced to

$$x_0(z_1) = 2\text{Re}\left(C_1C_2^*\right)b_{12}. \quad (24)$$

The propagation angle can also be expressed as

$$\alpha_x(z_1) = \frac{j}{k}\left(\iint C_1C_2^*u_{m_2n_2}\frac{\partial u_{m_1n_1}}{\partial x}dxdy - \\ \iint C_1^*C_2u_{m_1n_1}\frac{\partial u_{m_2n_2}}{\partial x}dxdy\right), \quad (25)$$

and reduced to

$$\alpha_x(z_1) = 2\text{Im}\left(C_1C_2^*\right)d_{12}. \quad (26)$$

The variables b_{12} and d_{12} are mode-specific integrals where

$$b_{12} = \iint xu_{m_1n_1}u_{m_2n_2}dxdy \quad (27)$$

and

$$d_{12} = \frac{-1}{k}\iint u_{m_2n_2}\frac{\partial u_{m_1n_1}}{\partial x}dxdy. \quad (28)$$

The offset and angle in the $\hat{y}$-direction is similarly found with $x \rightarrow y$ and $y \rightarrow x$. Note that an angle and offset only occur for modes where $m_2 = m_1 \pm 1$; in all other cases, b_{12} and d_{12} evaluate to zero.

Due to the dependence on real and imaginary parts of the complex magnitudes, it is seen that the offset and angle change with the beating, or phase difference, between modes as the fields propagate. It is useful to define the offset and tilt as sinusoidal functions dependent on z_1 by using Euler's identity such that,

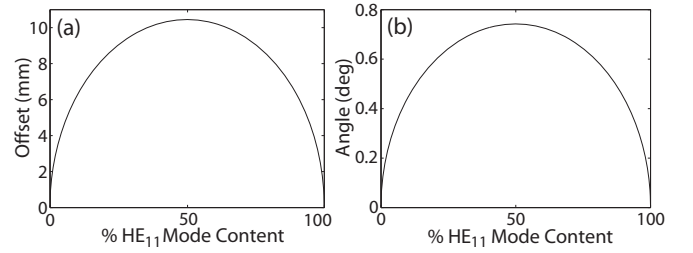$$x_0(z_1) = x_{max}\cos((\Delta k)z_1 + \theta_0) \quad (29)$$

Fig. 9. Maximum (a) offset and (b) tilt angle vs. HE_{11} percent content (A_p in Eq. (20)) for a combination of HE_{11} and LP_{11} modes.

$$\alpha_x(z_1) = -\alpha_{max}\sin((\Delta k)z_1 + \theta_0) \quad (30)$$

In this case, $(\Delta k)z_1$ indicates the phase difference between the modes and θ_0 is the phase difference at $z = 0$ between the modes. The maximum possible offset and angle for a combination of two modes are defined as

$$x_{max} = 2b_{12}|C_1C_2^*| \quad (31)$$

and

$$\alpha_{max} = 2d_{12}|C_1C_2^*|. \quad (32)$$

In addition, it can be inferred that x_{max} and α_{max} occur when $C_1C_2^*$ is either purely real or purely imaginary, respectively.

Eqs. (29) and (30), together with Eqs. (31) and (32) can be combined to form an expression for tilt and offset that is independent of location (z_1) on the transmission line. That is, the expression for tilt and offset may be combined to form a constant of the motion:

$$\left(\frac{x_0(z_1)}{b_{12}}\right)^2 + \left(\frac{\alpha_x(z_1)}{d_{12}}\right)^2 = 4|C_1C_2^*|^2. \quad (33)$$

The two governing parameters of the system are the percent split and phase difference between the two modes.

To illustrate this constant of the motion, we consider the common two mode combination of HE_{11} and $LP_{11}^{(e)}$ modes. In this case, b_{12} and d_{12} are evaluated as

$$b_{12} = \frac{\sqrt{2}}{a^2J_1(X_0)J_0(X_1)}\int_0^a J_0\left(\frac{X_0r}{a}\right)J_1\left(\frac{X_1r}{a}\right)r^2dr, \quad (34)$$

$$d_{12} = \frac{\lambda X_0 X_1}{\sqrt{2}\pi a\left(X_1^2 - X_0^2\right)}, \quad (35)$$

where $X_0 = 2.405$ and $X_1 = 3.832$, this gives $b_{12} = 0.329a$ and $d_{12} = 0.233\lambda/a$. For $a = 31.75$ cm and $\lambda = 1.76$ mm (170 GHz), these evaluate to $d_{12} = 0.74°$ and $b_{12} = 1.045$ cm. Figure 9 shows the maximum angle and offset for an input of these two modes as defined in Eq. (31) and (32) versus the percent split between the two modes, the only variable parameter which will change the maximum angle and offset. Figures 10 and 11 show the angle and offset due to an input with 80% HE_{11} and 20% LP_{11} or 90% HE_{11} and 10% LP_{11}, respectively, versus the phase difference between the modes, the second variable parameter. For these two modes, a phase difference of 2π corresponds to $z_1 = 5.07$ m. Due to interference effects, the power in the two modes propagates in the waveguide with sinusoidal oscillations in both tilt and offset, dependent on phase. By relation to the
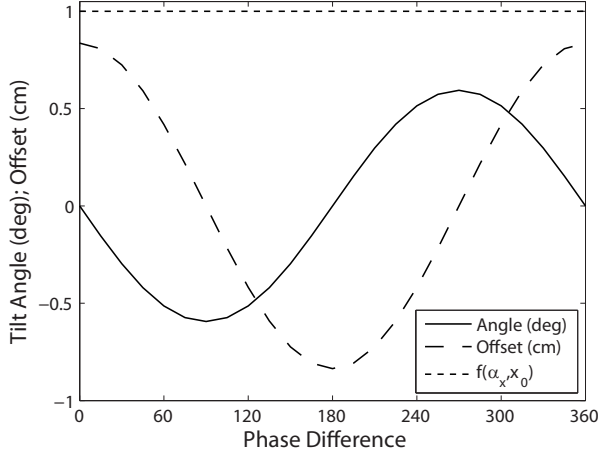
Fig. 10. The centroid offset and tilt angle for an input of 80% HE_{11} and 20% $LP_{11}^{(e)}$ in a waveguide of radius $a = 31.75$ mm at 170 GHz. $f(\alpha_x, x_0)$ plots Eq. 36. A 2π phase difference corresponds to $z_1 = 5.07$ m.
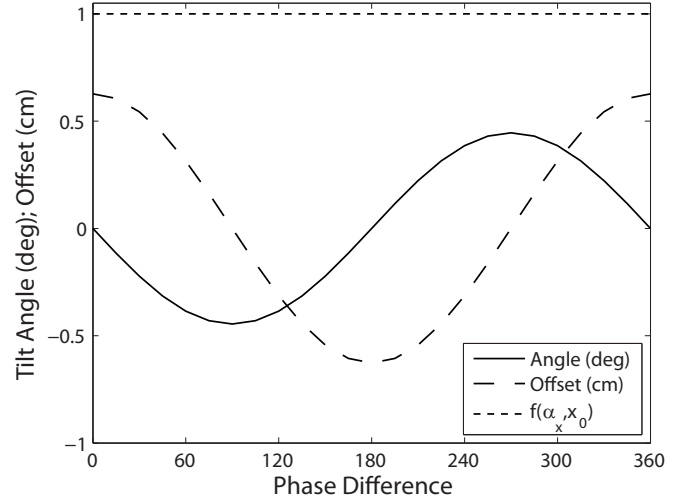

Fig. 11. The centroid offset and tilt angle for an input of 90% HE_{11} and 10% $LP_{11}^{(e)}$ in a waveguide of radius $a = 31.75$ mm at 170 GHz. $f(\alpha_x, x_0)$ plots Eq. 36. A 2π phase difference corresponds to $z_1 = 5.07$ m.

beat frequency between the two modes, the phase dependence can be quantified as the location in the waveguide where it is terminated and the wave is allowed to radiate into free space, $\theta = (\Delta k)z_1 + \theta_0$. Figure 10 has a larger split between the mode contents than Figure 11, causing a larger amplitude of offset and angle oscillations. In both figures, the oscillations are out of phase by $90°$ and combine (using (33)) to form a constant of the motion. In both figures we calculate $f(\alpha_x, x_0)$, where

$$ f(\alpha_x, x_0) = \frac{1}{4 \left| C_1 C_2^* \right|^2} \left[\left(\frac{x_0(z_1)}{b_{12}} \right)^2 + \left(\frac{\alpha_x(z_1)}{d_{12}} \right)^2 \right]. \quad (36) $$

and show that it is unity for all phases. Other percent splits between HE_{11} and LP_{11} will behave in the same pattern. In addition, other two-mode combinations that result in a centroid offset will behave similarly, i.e. modes that vary by one azimuthal index will follow the same pattern as the HE_{11} and LP_{11} combination illustrated here.

VII. DISCUSSION AND CONCLUSIONS

We have shown that the LP_{mn} modes form a convenient basis set for linearly polarized waves that are transmitted in large diameter, corrugated metallic waveguides with quarter-wave corrugations. The LP_{mn} modes may also be used to quantify the effects of HOMs in over-moded transmission lines. Applying this basis set to calculate the loss due to a gap in the waveguide for a pure mode input provides an assessment of the HOMs of the same azimuthal symmetry generated in a gap. An LP_{mn} mode at the input port of a gap generates HOMs at the output port with the same azimuthal symmetry (same m value). With a multiple mode input, the azimuthal symmetry of the problem reduces the complexity of analysis. For example, when considering the loss in a gap due to two modes, inputs which consist of HE_{11} and a higher order HE_{1n} mode will generate a phase dependence on HE_{11} loss. However, input with HE_{11} and LP_{mn} modes with $m > 0$ have a loss that is not dependent on phase. The phase between HE_{1n} modes causes a

swing in the HE_{11} power loss which increases with increasing HOM content, but the average loss in HE_{11} mode power over input HOM phases is not dependent on the amplitude of the HOM mode content.

The constant of motion for tilt and offset of a wave exiting a waveguide is useful in quantifying the effect of HOMs on transmission lines. This constant of motion relates the tilt and offset due to a particular two mode combination in the waveguide. For an angle and offset to occur, the two modes must be related such that the azimuthal indices vary by one, $m_2 = m_1 \pm 1$. The phase difference between modes modifies the split between centroid offset and propagation angle, but does not affect the constant of motion between the two parameters.

REFERENCES

[1] P. J. Clarricoats and A. D. Olver, "Low attenuation in corrugated circular waveguides," *Electronics Lett.*, vol. 9, no. 16, pp. 376–377, 1973.

[2] A. D. Olver, P. J. Clarricoats, and S. L. Chong, "Experimental determination of attenuation in corrugated circular waveguides," *Electronics Lett.*, vol. 9, no. 18, pp. 424–426, 1973.

[3] A. Cavallo, J. Doane, and R. Cutler, "Low-loss broadband multimode corrugated waveguide performance," *Rev. Sci. Instr.*, vol. 81, no. 9, pp. 2396–2400, 1990.

[4] M. K. Thumm and W. Kasparek, "Passive high-power microwave components," *IEEE Trans. Plasma Sci.*, vol. 30, no. 3, pp. 755–786, June 2002.

[5] J. L. Doane, "Propagation and Mode Coupling in Corrugated and Smooth-Wall Circular Waveguides," in *Infrared and Millimeter Waves, Vol. 13, Millimeter Components and Techniques Part IV*, K. J. Button, Ed. Academic Press, 1985, pp. 123–170.

[6] C. Dragone, "Attenuation and radiation characteristics of the HE_{11}-mode," *IEEE Trans. Microwave Theory and Techniques*, vol. 28, no. 7, pp. 704–710, 1980.

[7] J. P. Crenn and C. Charollais, "Propagation and Radiation Characteristics of the Circular Electric, Circular Magnetic, and Hybrid Waveguide Modes," *Int. J. Infrared and Millimeter Waves*, vol. 17, no. 9, pp. 1475–1506, 1996.

[8] E. Marcatili, "Hollow metallic and dielectric waveguides for long distance optical transmission and lasers," *Bell System Tech. J.*, vol. 43, pp. 1783–1809, 1964.

[9] P. J. Clarricoats and R. D. Elliot, "Multimode corrugated waveguide feed for monopulse radar," *IEEE Proc.*, vol. 128, no. 2, pp. 102–110, 1981.

[10] M. A. Henderson, B. Beckett, C. Darbos, N. Kobayashi, G. Saibene, F. Albajar, and T. Bonicelli, "A revised ITER EC system baseline design proposal," in *Proc. 15th Join Workshop on Electron Cyclotron Emission and Electron Cyclotron Resonance Heating*, J. Lohr, Ed.   World Scientific, 2009, pp. 453–484.

[11] R. A. Olstad, J. L. Doane, and C. P. Moeller, "Considerations in selection of ECH transmission line waveguide diameter for ITER," *3rd JAEA Tech. Meeting on ECRH Phys. and Tech. in ITER, J. Phys. Conf. Ser.*, vol. 25, pp. 166–171, 2005.

[12] R. J. Abrams, "Coupling Losses in Hollow Waveguide Laser Resonators," *IEEE J. Quantum Electronics*, vol. 50, no. 6, pp. 1526–1535, June 2002.

[13] K. Ohkubo, S. Kubo, H. Idei, M. Sato, T. Shimozuma, and Y. Takita, "Coupling of tilting Gaussian beam with hybrid mode in the corrugated waveguide," *Int. J. Infrared and Millimeter Waves*, vol. 18, no. 1, pp. 23–41, 1997.

[14] J. L. Degnan, "Waveguide laser mode patterns in the near and far field," *Appl. Optics*, vol. 12, no. 5, pp. 1026–1030, 1973.

[15] ——, "The waveguide laser: a review," *Appl. Phys.*, vol. 11, pp. 1–33, 1976.

[16] E. Marcatili, "Miter elbow for circular electric modes," in *Proc. Symp. on Quasi-Optics*.   Brooklyn, NY: Polytech Press, June 8–10, 1964, pp. 535–542.

[17] A. Yariv, *Optical Electronics*.   Philadelphia, PA: Saunders College Pub., 1991.

[18] J. L. Doane and C. P. Moeller, "HE_{11} mitre bends and gaps in a circular corrugated waveguide," *Int. J. Electronics*, vol. 77, pp. 489–509, 1994.

[19] D. Wagner, M. Thumm, K. Kasparek, G. A. Muller, and O. Braz, "Prediction of TE-, TM-, and hybrid-mode transmission losses in gaps of oversized waveguides using a scattering matrix code," *Int. J. Infrared and Millimeter Waves*, vol. 17, no. 6, pp. 1071–1081, 1996.

[20] A. G. Fox and T. Li, "Resonant Modes in a Maser Interferometer," *Bell System Tech. J.*, vol. 40, no. 2, pp. 453–488, 1961.